THE ASTROPHYSICAL JOURNAL, 450:L45–L49, 1995 September 10

LOW SURFACE BRIGHTNESS Hα OBSERVATIONS OF LOCAL INTERGALACTIC HYDROGEN CLOUDS[1]

MEGAN DONAHUE[2]
Space Telescope Science Institute, 3700 San Martin Drive, Baltimore, MD 21218
GREG ALDERING[2]
University of Minnesota, School of Physics and Astronomy, 116 Church Street, S. E., Minnesota, MN 55455
AND
JOHN T. STOCKE[2]
Center for Astrophysics and Space Astronomy, University of Colorado, Boulder, CO 80309-0391
Received 1995 February 7; accepted 1995 May 31

ABSTRACT

We present upper limits on the local ionizing background based on a search for extended Hα emission from three nearby intergalactic H I clouds: the Leo Ring (M96 group), both the NE and SW lobes of the Haynes-Giovanelli Virgo Cloud (H I 1225+01), and the H I tidal tails associated with the NGC 4631/4656 group. These clouds were chosen to have 21 cm emission that is extended (10–100 kpc) and distant from any associated galaxy. Deep, wide-field CCD images were acquired through narrow- (~31 Å) and broadband *R* filters with the Burrell Schmidt telescope on Kitt Peak. We set a 95% confidence upper limit on the Hα surface brightness for the areas of the clouds detected in H I of 1.6×10^{-19} ergs s^{-1} cm^{-2} arcsec^{-2} in Leo and of 3.7×10^{-19} ergs s^{-1} cm^{-2} arcsec^{-2} in Virgo. We limit the local ionizing background to $\Phi_0 < 5.0 \times 10^3$ photons s^{-1} cm^{-2} sr^{-1} (95%) at the location of the Leo Ring cloud and $\Phi_0 < 1.1 \times 10^4$ photons s^{-1} cm^{-2} sr^{-1} at the Virgo cloud, assuming spherical clouds. (Limits are a factor of 2 higher for a thin face-on slab.) The limits correspond to $J_0 < 3.3 \times 10^{-23}$ and 7.6×10^{-23} ergs s^{-1} cm^{-2} sr^{-1} Hz^{-1} for a $\nu^{-1/2}$ spectrum (1.6 times higher for a $\nu^{-1.4}$ spectrum) between 1 and 4 ryd. Such low limits suggest that quasar light, and not galactic light, dominates the ionizing background at low redshift. The Hα limit on the Leo cloud is significantly below a previously reported detection. In the field of the edge-on galaxies NGC 4631 and NGC 4656, we detect Hα from ionized gas extending nearly 16 kpc above N4631, which could have been blown out by starburst activity in the plane, and a low surface brightness companion or stellar tidal tail. This companion lies between N4631's H I tidal tails and may have played a role in creating the H I tidal tails, or it may represent star formation within the tidal tails. We also report the tentative detection of an ultrafaint "sheet" of Hα emission extending from NGC 4631 to NGC 4656.

Subject heading: intergalactic medium

1. INTRODUCTION

In this letter, we present results from our narrow-band Hα imaging survey of several intergalactic H I clouds. These results place interesting limits on the level of the local metagalactic background radiation field at wavelengths <912 Å. Since our own Galaxy is optically thick in all directions to radiation between 1 and 4 ryd (1 ryd = 13.6 eV), this important radiation field cannot be measured directly. Only indirect methods can reveal the magnitude of the ionizing radiation background.[3] For example, the deficit in the number of Lyα absorption features is used to estimate the quasar's sphere of influence (Bajtlik, Duncan, & Ostriker 1988). Estimates from this "proximity effect" at high redshift are typically $J_0 \sim 10^{-21}$ ergs s^{-1} cm^{-2} sr^{-1} Hz^{-1} (Bechtold 1994; Lu, Wolfe, & Turnshek 1991; Bajtlik et al. 1988). Locally, the proximity effect in Lyα forest absorption systems in the *Hubble Space Telescope* (*HST*) spectra of nearby quasars gives a 1 σ (65% confidence) range of 0.2–3.6 × 10^{-23} ergs s^{-1} cm^{-2} sr^{-1} Hz^{-1} (Kulkarni & Fall 1993). Extrapolation from rocket-borne experiments of the far-UV background at 1200 Å to 912 Å give $J_0 < 6 \times 10^{-22}$ ergs s^{-1} cm^{-2} sr^{-1} Hz^{-1} (Holberg 1986; Martin, Hurwitz, & Bowyer 1991). J_0 from only quasars and active galactic nuclei (AGNs) is between 1–20 × 10^{-23} ergs s^{-1} cm^{-2} sr^{-1} Hz^{-1}, with assumptions about local quasar luminosity functions, intrinsic spectral shapes, and radiative transfer through the diffuse intergalactic medium and the Lyα absorption clouds (Miralda-Escudé & Ostriker 1990; Madau 1992; Terasawa 1992; Lin & Phinney 1993; Meiksin & Madau 1993). Bochkarev & Sunyaev (1977) suggested that photoionization by the metagalactic background could cause sharp edges in the neutral hydrogen disks of spiral galaxies, and that the structure of those edges is modified by the intensity and spectrum of the metagalactic background. Models of the H I drop-off observed in NGC 3198 (van Gorkom 1993) suggest $J_0 \sim 1$–10×10^{-23} ergs s^{-1} cm^{-2} sr^{-1} Hz^{-1} (Maloney 1993; Dove & Shull 1994; Corbelli & Salpeter 1993). Models of the evolution with redshift of the number density of Lyα absorbers in quasar spectra assume that the ionizing background drives the evolution of the absorbers and that the ionizing background at high redshift (z = 2–4) is measured by the proximity effect ($J_0 \sim 10^{-21}$ ergs s^{-1} cm^{-2} sr^{-1} Hz^{-1}.) For these models, local estimates of the ionizing background tend to be between 10^{-23} ergs s^{-1} cm^{-2}

[1] Observations were made with the Burrell Schmidt telescope at the Warner and Swasey Observatory, Case Western Reserve University.
[2] Visiting Astronomer, National Optical Astronomy Observatories, Tucson, AZ.
[3] In this paper, we quantify the ionizing background in terms of specific intensity at 1 ryd equal to J_0 in ergs s^{-1} cm^{-2} sr^{-1} Hz^{-1} and in units of photon flux Φ_0 in photons s^{-1} cm^{-2} sr^{-1}. Both derived quantities depend on the geometry of the absorber, but Φ_0 is independent of the shape of the ionizing spectrum.

sr^{-1} Hz^{-1} (Ikeuchi & Turner 1991) and 2×10^{-22} ergs s^{-1} cm^{-2} sr^{-1} Hz^{-1} (Murakami & Ikeuchi 1994).

Measuring the recombination radiation from intergalactic H I clouds is the most direct and assumption-free method of assessing the metagalactic ionizing radiation field. Several attempts have been made to measure the Hα surface brightness of intergalactic clouds, including the Galactic "high-velocity" clouds (Kutyrev & Reynolds 1989; Songaila, Bryant, & Cowie 1989). Galactic high-velocity clouds may well be dominated by internal sources of photoionization (e.g., Veilleux, Cecil, & Bland-Hawthorn 1995), photoionized by intergalactic radiation on only one side, or completely shielded by the Reynolds layer and not exposed to intergalactic radiation at all. Therefore, for the purposes of estimating the ionizing background, observations of truly intergalactic H I clouds are superior to those of Galactic high-velocity clouds. The most recent and sensitive Fabry-Perot measurements of an intergalactic cloud in Virgo give 2 σ upper limits of $\sim 8 \times 10^{-23}$ ergs s^{-1} cm^{-2} sr^{-1} Hz^{-1} (Vogel et al. 1995) from an Hα surface brightness limit of 1.1×10^{-19} ergs s^{-1} cm^{-2} $arcsec^{-2}$. Previously Reynolds et al. (1986) had reported a 4 σ detection of Hα from the "Leo Ring" cloud (Schneider et al. 1983), implying $J_0 \sim 3 \times 10^{-22}$ ergs s^{-1} cm^{-2} sr^{-1} Hz^{-1}. Here we report faint limits on the surface brightness in Hα of extragalactic hydrogen clouds obtained from narrow-band filter imaging of the area on the sky defined by the contours of 21 cm emission from the clouds, and we report an unexpected detection of Hα emission at large distances from the edge-on galaxies NGC 4631 and NGC 4656.

2. OBSERVATIONS AND DATA ANALYSIS

CCD images of three nearby extragalactic neutral hydrogen clouds were obtained with the 24 inch (61 cm) Case Western Burrell Schmidt located on Kitt Peak. These clouds are the Leo Ring in the M96 group of galaxies, the H I clouds associated with the galaxies NGC 4631 and NGC 4656, and both the NE and SW lobes of an extragalactic cloud in Virgo discovered by Giovanelli & Haynes (1989), H I 1225+01. All systems have excellent 21 cm H I maps. The Leo Ring in the M96 group (discovered by Schneider et al. 1983) was observed recently by Schneider et al. (1989). The NGC 4631/NGC 4656 system was observed most recently by Rand & van der Hulst (1993; also Weliachew, Sancisi, & Guelin 1978) and Rand (1994). Giovanelli et al. (1991) reobserved the Virgo cloud and resolved its H I system into two lobes. A low surface brightness Hα galaxy occupies the northeast lobe; the southwest component, of nearly the same column density, has no obvious optical counterpart (Salzer et al. 1991). The radial velocities of the clouds fell within the range 400–1800 km s^{-1}, so a single narrow-band filter encompasses the potential Hα emission from all the clouds.

We took multiple broadband *R* and narrow-band (31 Å FWHM) Hα exposures of each cloud system, manually moving the telescope by 10′–15′ between exposures. We used the CCD ST2K (2048×2048 pixels) with a read noise of 3 electrons and gain of 0.89 and 0.94 electrons per analog-to-digital converter unit (ADU) for two observing runs at KPNO (1993 March and 1994 March). The data from 1994 March were superior in quality as a result of weather, a newly installed automatic filter wheel, a new shutter, and improved light control inside the dome. The results we report in this Letter are drawn entirely from this superior data set. The bandpass of the narrow-band filter is centered on 6583 Å with a FWHM of 31 Å after including the effects of the f/3.6 converging beam of the Burrell Schmidt and accounting for the dome air temperature. This corresponds to a velocity range of ~400–1800 km s^{-1} for Hα. We reduced and analyzed the data with IRAF (v2.10.3) and modified FOCAS routines.

The field of view was nearly 1° square with a plate scale of 2.″028 $pixel^{-1}$ (confirmed by astrometric measurements of the M67 field). We obtained 11–15 bias frames at the beginning and end of each night, and several 1 hr dark exposures. The object exposures were long enough to be dominated by sky noise. A constant overscan bias was subtracted from each image. We found no significant changes in the two-dimensional structure of the bias and dark frames from night to night, so we constructed a single mean bias and dark image which were subtracted from each frame. These zero-level corrections had no significant spatial structure except near a bad column, so they did not affect our measurements substantially. In order to co-add object frames to create a super–sky flat for each filter, bright objects in the individual frames were identified in FOCAS and masked out. Typically a region having twice the inital FOCAS detection area was masked to ensure elimination of flux greater than ~0.1% of sky. This data set required only one iteration through this procedure. Individual frames were flattened by the final version of the super sky flat, then co-added into an image in each filter for each target field. The images were aligned to within 1 pixel with no interpolation of pixel values.

To obtain an unbiased mean sky value and to optimize the detection of low surface brightness, extended objects, bright objects including stars and galaxies were excluded from the co-added image with the object masks. A secondary mask was made from the co-added image to remove fainter features such as diffraction spikes of bright stars. A final image was constructed by co-adding the masked images of the appropriate field, multiplicatively scaled and weighted by the relative image-to-image photometry of stars on the individual fields, and a constant zero offset added to match the sky level image-to-image. Cosmic rays were rejected with a "ccdclip" algorithm, which uses the noise characteristics of the chip to reject individual pixels. (Experiments with point-spread function fitting and star subtraction in IRAF/DAOPHOT resulted in inferior sky images.) The stellar images were significantly undersampled; therefore, perfect cosmic-ray rejection and stellar photometry on the final image is impossible. Extended objects are not affected.

For each field, the resultant sky image was median-filtered on large scales ($2.'24 \times 2.'24$) by binning the pixels contained in this region into a histogram of 600,000 bins, and using the median of this distribution as the new value of the output image pixel. The resulting flatness of the sky in the median-filtered images was excellent—about 5×10^{-4} over scales of arcminutes. This noise level is only ~25% higher than what would be expected from photon statistics.

We measured the mean sky brightness in approximately 20 boxes on the cloud and 20 boxes off the cloud. The boxes were $2' \times 2'$ in size. These boxes were chosen by eye to avoid areas contaminated by low surface brightness features from galaxies and scattering halos from bright stars. We then computed the standard error of the difference of the means between on-cloud and off-cloud samples (Press et al. 1986, eq. [13.4.1]) and determined from a Student *t*-test that the means were not significantly different for either the Leo or Virgo fields (Press

TABLE 1

OBSERVING DATA

H I Cloud	Dates	Filter	Time per frame (s)	Number of frames	Calibration[a]
Leo Ring	1994 Mar 13, 16–17	Hα	900	22	10.9
NGC 4631/NGC 4656	1994 Mar 13, 16	Hα	900	15	12.4
Virgo	1994 Mar 17, 18	Hα	900	13	12.1
NGC 4631/NGC 4656	1994 Mar 13	R	500	13	
Leo Ring	1994 Mar 13	R	500	13	
Blank field	1994 Mar 16	R	900	9	

[a] The equivalent conversion of 1 ADU s^{-1} in units of photons s^{-1}. The *R*-band conversion is stated in the text.

et al. 1986, pp. 464–468). The 95th percentile confidence limits were computed with Student's *t*-test (Press et al. 1986). The mean measurements and limits are reported in Table 2.

The images were calibrated with observations of the standard star BD+332624, observed with the same setup. The calibration of the 6583/31 Å filter indicates that 1 ADU s^{-1} was equivalent to about 11 photons s^{-1} above the atmosphere. Specific conversions for the range of 21 cm velocities for each cloud are listed in Table 1. All the Hα exposures were 900 s in length, so for a mean sky image, 1 ADU per pixel per 900 s corresponds to 4.33×10^4 photons s^{-1} cm^{-2} sr^{-1}, which is equal to 540 mR, an emission measure of 1.50 cm^{-6} pc, or a surface brightness of 3.09×10^{-18} ergs s^{-1} cm^{-2} $arcsec^{-2}$.

To subtract the continuum contribution from the Hα images, we also obtained and reduced broadband *R* (Harris *R*) images in a similar fashion. Since we detected Hα in only one field (NGC 4631/NGC 4656), continuum subtraction was done only for that field. We calibrated the *R* images with 40 stars in SA 107 taken from Landolt (1992) and found $R = 21.37 - 2.5 \log (\text{ADU s}^{-1}) - 0.20(X - 1.23)$, where X is air mass. We converted surface brightness to physical units (ergs s^{-1} cm^{-2} sr^{-1} Hz^{-1}) using the calibration of Bessel (1979). After median-filtering both images, the *R* image was scaled according to the calibration. We checked this scaling by comparing stellar fluxes in the two best individual *R*-band and Hα images. The stellar ratios were consistent with the calibration ratios. The scatter in the stellar ratios was ±10%. The scaled red image was subtracted from the Hα image of NGC 4631/NGC 4656.

3. LIMITS ON THE LOCAL METAGALACTIC IONIZING FLUX

The surface brightness of an optically thick neutral hydrogen cloud is directly proportional to the ionizing photon flux incident on that cloud. We assume that the cloud is optically thin to Hα photons and illuminated on all sides, and so we count photons from both sides of the cloud. The exact flux from a cloud depends on its geometry; specifically, the ratio of its surface area to the projected cloud area (Stocke et al. 1991). If we assume case B recombination at $\sim 10^4$ K (Osterbrock 1989), ~45% of the incident ionizing photons are converted to Hα photons. Therefore, the value of the metagalactic ionizing background at 1 ryd (J_0 at 13.6 eV) is approximately $\Phi_0 = f_g \Phi_{\text{H}\alpha}/0.45$, or

$$J_0 = \frac{h\Phi_{\text{H}\alpha}}{f_{\text{H}\alpha}} f_g f_s = 1.47 \times 10^{-26} f_g f_s \Phi_{\text{H}\alpha}, \quad (1)$$

where J_0 is in ergs s^{-1} cm^{-2} sr^{-1} Hz^{-1}, h is Planck's constant, $\Phi_{\text{H}\alpha}$ is the photon surface brightness of Hα in photons s^{-1} cm^{-2} sr^{-1}, $f_{\text{H}\alpha} \approx 0.45$, f_s is the adjustment for spectral shape between 1 and 4 ryd, and f_g is the geometrical correction factor. The value of f_g is 1 for a sphere, $4/\pi$ for a long, narrow cylinder, 2 for a face-on slab (see also Stocke et al. 1991), and $[2 \cos (\Theta)]$ for a slab inclined at an angle Θ with respect to the observer. In Table 2, we report 95% confidence level upper limits on Φ_0, which is independent of the incident radiation spectral index, and on J_0 assuming spherical clouds and spectral index $s = 0.5$ (except for NGC 4631/NGC 4656, where we have a detection). The highest energy photons will either pass on through or be absorbed by heavier elements. We approximate this effect by assuming that only photons between 1 and 4 ryd are absorbed by hydrogen atoms. If $J_\nu = J_0(\nu/\nu_0)^{-s}$, where $s \geq 0$ between 1 and 4 ryd, then for a flat spectrum ($s = 0$), $f_s = \ln(4)^{-1}$, or for $s > 0$, $f_s = s/(1 - 4^{-s})$. For $s = 0$–1.4, multiply the Table 2 estimate for J_0 by $f_s = 0.72$–1.63.

4. DETECTION OF EXTENDED Hα ASSOCIATED WITH NGC 4631

NGC 4631 is a nearby edge-on galaxy known for its high level of star formation. The galaxy group NGC 4631/NGC 4656 has been observed in Hα before (Rand, Kulkarni, & Hester 1992, sensitive to 3.2 pc cm^{-6}), but never to this depth.

TABLE 2

SKY SIGMA AND LIMITING SKY SURFACE BRIGHTNESS

Name	Mean Sky (ADU)	σ (rms)[a] (ADU)	95%[b] (ADU)	Hα[c]	Φ_0[d]	J_0[e]
Leo cloud	128.68	0.108	0.054	1.62 (−19)	5060	3.34 (−23)
Virgo cloud	169.91	0.224	0.106	3.68 (−19)	11500	7.62 (−23)
NGC 4631/NGC 4656	128.90	0.07	...	...	...	...

[a] Root mean square deviation from the mean for in a sample of 2′ by 2′ boxes.
[b] 95th percentile confidence level from a Student's *t*-test on the difference between the mean sky and cloud surface brightnesses. The units are ADU $pixel^{-1}$ $(900\ s)^{-1}$.
[c] Units are ergs s^{-1} cm^{-2} $arcsec^{-2}$.
[d] Units are photons s^{-1} cm^{-2} sr^{-1}.
[e] Units are ergs s^{-1} cm^{-2} sr^{-1} Hz^{-1}.

Our surface brightness sensitivity of <0.3 cm^{-6} pc is much lower than previous Hα observations of other edge-on spirals (Pildis, Bregman, & Schombert 1994: 19 cm^{-6} pc.) We draw the reader's attention to newly discovered Hα emission in three regions: extended Hα emission along the minor axes of NGC 4631 and NGC 4656, above and below the disk (but not as highly flattened as the H I); an apparent companion galaxy or tidal feature associated with NGC 4631; and faint, possibly scattered, light extending in a sheet between NGC 4631 and NGC 4656 (See Fig. 1 [Pl. L5]). The apparent companion or tidal feature is a finger-like structure lying between the two tidal H I tails and is clearly detected in continuum broadband images. This structure may be a tidal extension of NGC 4631 or it may be a small satellite galaxy, perhaps distorting the H I component of NGC 4631. After subtracting the continuum contribution from the satellite galaxy, the peak Hα surface brightness in the region of the satellite galaxy to NGC 4631 is $<1.4 \times 10^{-18}$ ergs s^{-1} cm^{-2} arcsec^{-2}. This upper limit arises from the uncertainty in the continuum subtraction. If this extended emission "sheet" between the galaxies arises from photoionization by the metagalactic background, $J_0 \sim 2$–3×10^{-22} ergs s^{-1} cm^{-2} sr^{-1} Hz^{-1}, a factor of 10 higher than the upper limit in the Leo field. Since we did not detect extended Hα in the Leo field, which had very similar sensitivity, the Hα detected in the halo or the extended sheet in the field of NGC 4631 likely does not arise from photoionization from a metagalactic ionizing background, but rather from local sources. Indeed, the Hα features associated directly with halos of the two galaxies have all the hallmarks of a superwind blowout.

The strongly asymmetric shape of the NGC 4631 and NGC 4656 halos, and the good subtraction of the field stars, indicates that scattered light (in the telescope optics) is at best a minor component of the Hα galaxy halos we observe. To check this, we constructed a point-spread function from the halos of saturated stars and the central cores of nonsaturated stars. The final image containing NGC 4631 and foreground stars was deconvolved with a Lucy-Richardson algorithm (Lucy 1974; Richardson 1972). We then treated this image identically to the original image, masking out the stars and the galaxies, smoothing on scales of 2′ by 2′, then subtracting the scaled and smoothed red image from it. The extended sheet-like structure develops some lumpiness, but the halos and companion galaxy remained unchanged in structure. It is extremely unlikely that an unusual *R*-band to Hα ratio for stars in the halos of NGC 4631 and NGC 4656 could produce the features seen in the difference image. The halo "starburst" feature is the most robust: no possible combination of continuum and emission-line image can subtract this feature, since it is clearly morphologically distinct. Thus, we are confident that scattered light and color effects cannot reproduce the halo and companion galaxy features, but scattered light may contribute to the large-scale "sheet" extending from NGC 4631 to NGC 4656.

NGC 4631 has soft X-ray emission extending 8 kpc north of the midplane of the galaxy (Wang et al. 1995), and its radio continuum halo (Ekers & Sancisi 1977) has the largest *z*-extent ($\gtrsim$10 kpc) of all known late-type spiral galaxies. The Hα emission extends at least 8.′2 from the center of the galaxy. At a distance of 6.9 Mpc (Tully 1988), this corresponds to 16.5 kpc. Therefore, we detect Hα to larger altitudes above the disk than the X-ray and radio emission. We defer a detailed analysis of NGC 4631 to a future paper.

5. DISCUSSION

Recent Fabry-Perot observations by Vogel et al. (1995) report stringent upper limits on the surface brightness of Hα from the NW lobe of H I 1225+01. Their upper limits for Hα from this cloud are somewhat deeper than those we report here for the same cloud, but our upper limit for Leo is very similar. Narrow-band observing with the Schmidt CCD camera accesses a wider field of view than most Fabry-Perot instruments, but the FP is able to probe the spectral dimension with higher resolution, and hence lower sky flux, than narrow-band imaging. This advantage usually sacrifices the ability to simultaneously measure cloud and sky over a large solid angle as is possible with narrow-band imaging. Both methods are are still in the photon-limited regime, so even better limits should be possible with longer integrations. Certainly both methods should be used to confirm detections, since, for example, our upper limit for the Leo cloud lies well below the reported detection of Hα by a Fabry-Perot instrument (Reynolds et al. 1986).

Our upper limit of $J_0 < 3 f_s f_g \times 10^{-23}$ ergs s^{-1} cm^{-2} sr^{-1} Hz^{-1} and that of Vogel et al. (1995) restricts the contribution of classes of sources to the ionizing background. Madau (1992) calculates that the quasar contribution to the ionizing background at $z = 0$ is 5–6×10^{-24} ergs s^{-1} cm^{-2} sr^{-1} Hz^{-1}, independent of assumptions about quasi-stellar object evolution and attenuation by intervening absorption systems. These estimates are similar to other models (Miralda-Escudé & Ostriker 1990, 1992). Therefore, our observed limits constrain the amount of background light that can be contributed by *other* sources of photoionization such as the population of faint blue galaxies. Meiksin & Madau (1993, hereafter MM93) calculate the contribution of flat-spectrum galaxies to the *B*-band background light at $z = 0$ to be 2.4×10^{-21} ergs s^{-1} cm^{-2} sr^{-1} Hz^{-1}. Using the formula in MM93 and assuming that the blue galaxies turn on at a redshift of 1, the current epoch $J_0 = 2$–$5.5 \times 10^{-22} f_*$ ergs s^{-1} cm^{-2} sr^{-1} Hz^{-1}, where f_* is the fraction of blue galaxies forming stars multiplied by the escape fraction of ionizing light from the galaxy. If blue galaxies supplied *all* the background (which is clearly an overestimate), $f_* < 0.13 - 0.05(f_s f_g)$. Our lower limits suggest that the ionizing background light is dominated by quasars and not galaxies.

Finally, we have detected Hα emission at larger distances above a galactic disk than ever before observed ($\geq$15 kpc) (see Dettmar 1992 for a review). We also detect Hα emission at even larger scales that is probably associated with tidal interactions. All such gas significantly enhances the cross section of galaxies for hydrogen and/or metal absorption lines along the line of sight. Perhaps some of the local Lyα absorption lines at low redshifts (Bahcall et al. 1993; Morris et al. 1991) are associated with ionized gas that is distant from, but associated with, galaxies (Morris et al. 1993; Mo & Morris 1994). Rather than extended hydrogen disks photoionized by an ambient background (e.g., Maloney 1992), the gas may have been blown out perpendicularly to the disks or tidally torn out to large radii. The system NGC 4631/NGC 4656 shows evidence for both processes, creating a gaseous cross section of at least 43.′4 $\times$ 37.′2 (87×75 kpc^2). These gaseous halos would need to extend at least 10 times farther at $N_{\rm H\,I} \sim 10^{13-14}$ cm^{-2} to explain all the Lyα absorption-line detections (Stocke et al. 1995), but they are are similar to sizes inferred for Mg II quasar absorption-line systems (e.g., Bergeron et al. 1994; Bergeron, Cristiani, & Shaver 1992; Srianand & Khare 1994). Note that

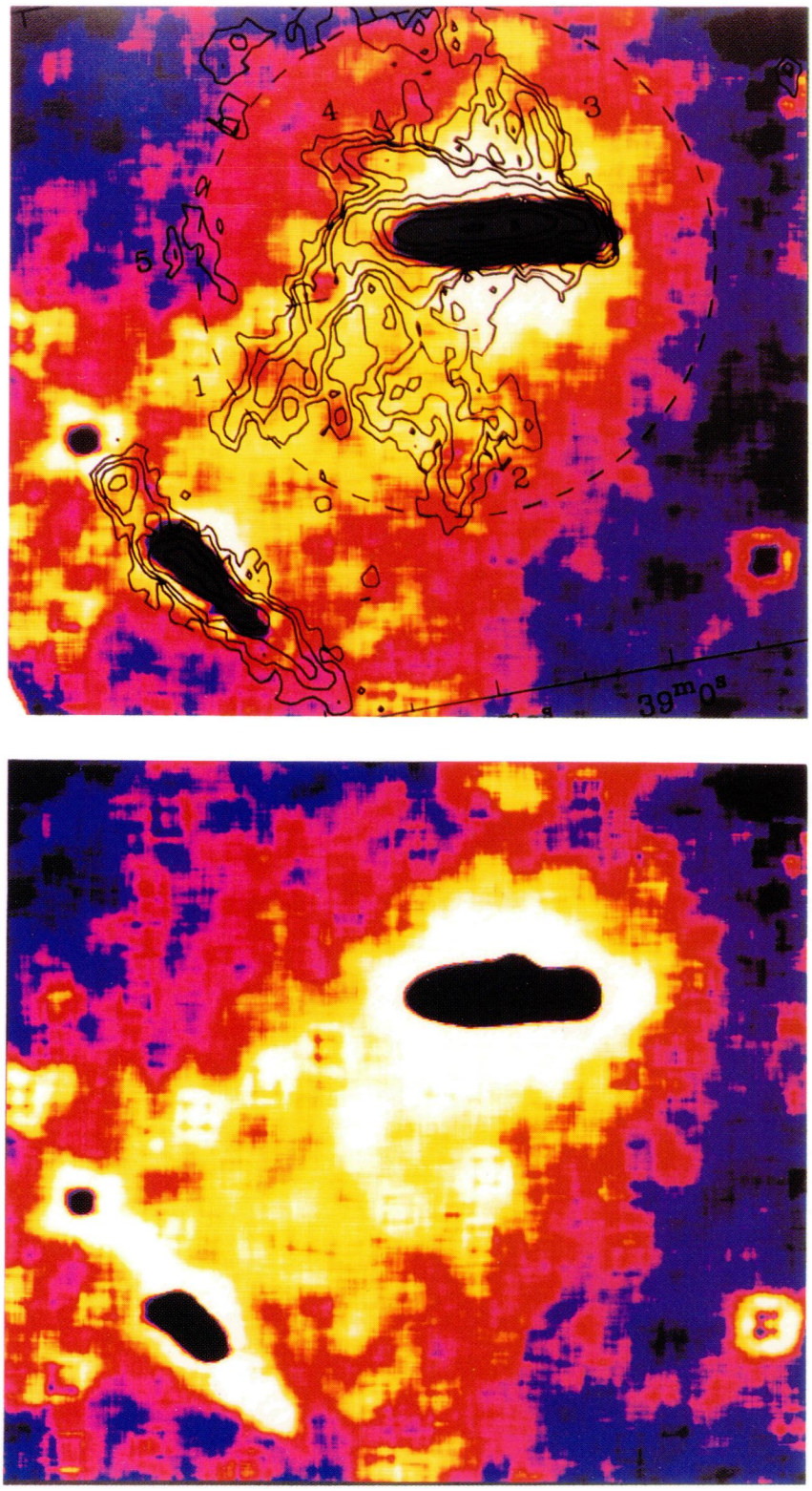

FIG. 1.—*Bottom*: an Hα + continuum false-color image of NGC 4631/NGC 4656, with NGC 4631 at the top of the image and NGC 4656 in the lower left corner. Each image is 50.′8 by 57.′5. North is toward the top, and East is to the left in both images. The stars and the central brightest portions of the galaxies have been masked out of the images, and the images were smoothed with a 2′ × 2′ median filter (see text for details). A tidal feature or low surface brightness galaxy is apparent in yellow between the NGC 4631 and NGC 4656 and lies between two H I spurs. Faint scattering halos around a few of the brightest stars are visible as square structures on the median-filtered image, particularly just north of spur 1 (defined in Rand & van der Hulst 1993 and labeled on the contour overlay). *Top*: a pure Hα image of NGC 4631/NGC 4656, with the H I contour map of Rand (1994) approximately aligned and superimposed. Relatively bright ionized gas, with emission measure of ~2.2–1.1 cm^{-6} pc (coded white) extends nearly 16 kpc from the midpoint of NGC 4631 and also extends away from NGC 4656 on the NW side, near the location of the H I spur in its H I distribution. The extended light "sheet" between the galaxies has an approximate emission measure of ~0.3 cm^{-6} pc (coded yellow) and may be somewhat contaminated by stellar light scattered by telescope optics.

this is only the cross section of gas that is relatively opaque to ionizing photons ($N_{\rm H\,I} \gtrsim 10^{18}$ cm^{-2}) and that the intersection cross section of gas with lower column density (relevant to Lyα clouds with $N_{\rm H\,I} \sim 10^{13}$–$10^{14}$ cm^{-2}) is probably much larger, albeit impossible to detect in emission.

M. D. and G. A. were supported by Carnegie Fellowships. G. A. also acknowledges support from the University of Minnesota. J. T. S. was supported by NSF grant AST-9020008. We thank Ed Carder for providing tracings of the narrow-band filter. Richard Rand kindly supplied an improved H I contour map of NGC 4631/4656. Funding from the Observatory of the Carnegie Institution of Washington in Pasadena director's discretionary fund paid for the narrow-band filter. We thank Mark Voit and the referee Stuart Vogel for reviewing the radiative transfer calculations.

REFERENCES

Bahcall, J. N., et al. 1993, ApJS, 87, 1
Bajtlik, S., Duncan, R. C., & Ostriker, J. P. 1988, ApJ, 327, 570
Bechtold, J. 1994, ApJS, 91, 1
Bergeron, J., et al. 1994, ApJ, 436, 33
Bergeron, J., Cristiani, S., & Shaver, P. A. 1992, AA, 257, 417
Bessel, M. S. 1979, PASP, 91, 589
Bochkarev, N. G., & Sunyaev, R. A. 1977, Astron. Zh., 54, 957; translated in Soviet Astron., 21, 542
Corbelli, E., & Salpeter, E. E. 1993, ApJ, 419, 104
Dettmar, R.-J. 1992, Fundam. Cosmic Phys., 15, 143
Dove, J. B., & Shull, J. M. 1994, ApJ, 423, 196
Ekers, R. D., & Sancisi, R. 1977, AA, 54, 973
Giovanelli, R., & Haynes, M. P. 1989, ApJ, 346, L5
Giovanelli, R., et al. 1991, AJ, 101, 1242
Holberg, J. B. 1986, ApJ, 311, 969
Ikeuchi, S., & Turner, E. L. 1991, ApJ, 381, L1
Kulkarni, V. P., & Fall, S. M. 1993, ApJ, 413, L63
Kutyrev, A. S., & Reynolds, R. J. 1989, ApJ, 344, L9
Landolt, A. U. 1992, AJ, 104, 340
Lin, Z., & Phinney, E. S. 1993, ApJ, 418, 28
Lu, L., Wolfe, A. M., & Turnshek, D. A. 1991, ApJ, 367, 19
Lucy, L. B. 1974, AJ, 79, 745
Madau, P. 1992, ApJ, 389, L1
Maloney, P. 1993, ApJ, 414, 41
———. 1992, ApJ, 398, L89
Martin, C., Hurwitz, M., & Bowyer, S. 1991, ApJ, 379, 549
Meiksin, A., & Madau, P. 1993, ApJ, 412, 34 (MM93)
Miralda-Escudé, J., & Ostriker, J. P. 1990, ApJ, 350, 1
———. 1992, ApJ, 392, 15
Mo, H. J., & Morris, S. L. 1994, MNRAS, 269, 52
Morris, S. L., Weymann, R. J., Dressler, A., McCarthy, P. J., Smith, B. A., Terrile, R. J., Giovanelli, R., & Irwin, M. 1993, ApJ, 419, 524
Morris, S. L., Weymann, R. J., Savage, D. B., & Gilliland, R. L. 1991, ApJ, 377, L21
Murakami, I., & Ikeuchi, S. 1994, 421, L79
Osterbrock, D. E. 1989, Astrophysics of Gaseous Nebulae and Active Galactic Nuclei, (Mill Valley, CA: University Science Books)
Pierce, M. J., & Tully, R. B. 1985, AJ, 90, 450
Pildis, R. A., Bregman, J. N., & Schombert, J. M. 1994, ApJ, 427, 160
Press, W. H., Flannery, B. P., Teukolsky, S. A., & Vetterling, W. T. 1986, Numerical Recipes (Cambridge: Cambridge Univ. Press)
Rand, R. 1994, A&A, 285, 833
Rand, R., Kulkarni, S. J., & Hester, J. J. 1992, ApJ, 396, 97
Rand, R., & van der Hulst, J. M. 1993, AJ, 105, 2098
Reynolds, R. J., Magee, K., Roesler, F. L., Scherb, F., & Harlander, J., 1986, ApJ, 309, L9
Richardson, W. H. 1972, J. Opt. Soc. Am., 62, 55
Salzer, J. J., di Serego Alighieri, S., Matteuchi, F., Giovanelli, R., & Haynes, M. P. 1991, AJ, 101, 1258
Schneider, S. E., et al. 1989, AJ, 97, 666
Schneider, S. E., Helou, G., Salpeter, E. E., & Terzian, Y. 1983, ApJ, 273, L1
Songaila, A., Bryant, W., & Cowie, L. L. 1989, ApJ, 345, L71
Srianand, R., & Khare, P. 1994, ApJ, 428, 82
Stocke, J. T., Case, J., Donahue, M., Shull, J. M., & Snow, T. P. 1991, ApJ, 374, 72
Stocke, J. T., Shull, J. M., Penton, S., Donahue, M., & Carilli, C. 1995, ApJ, in press
Terasawa, N. 1992, ApJ, 392, L15
Tully, B. 1988, Nearby Galaxies Catalog (Cambridge: Cambridge Univ. Press)
van Gorkom, J. H. 1993, in The Environment and Evolution of Galaxies, ed. J. M. Shull & H. A. Thronson (Dordrecht: Kluwer), 345 (includes reference to van Gorkom, J. H., et al. 1995, in preparation)
Veilleux, S., Cecil, G., & Bland-Hawthorn, J. 1995, ApJ, 445, 152
Vogel, S., Weymann, R., Rauch, M., & Hamilton, T. 1995, ApJ, 441, 162
Wang, Q. D., Walterbos, R. A. M., Steakley, M. F., Norman, C. A., & Braun, R. 1995, ApJ, 439, 176
Weliachew, L., Sancisi, R., & Guélin, M. 1978, A&A, 65, 37